

# Innovation

## A New Approach to an Old Problem

# Carrier-Phase Cycle Slips

**Sunil B. Bisnath, Donghyun Kim, and Richard B. Langley**  
University of New Brunswick

*High-precision GPS positioning and navigation requires that the data preprocessing stage correctly repair cycle slips in the carrier-phase observations. A slip of only a few cycles can bias measurements enough to make centimeter-level positioning or navigation difficult. Over the past decade, researchers have developed numerous methods to detect and repair cycle slips. Yet, invariably, a few cycle slips remain undetected or incorrectly repaired, requiring analyst intervention to fully clean up the data. A perfectly operating, automated GPS data preprocessor remains an elusive goal. However, two of my colleagues at the University of New Brunswick, Sunil Bisnath and Donghyun Kim, have developed a technique that advances preprocessor capability significantly, and they join me in describing their work in this month's column. Sunil Bisnath received a B.Sc. (Hons.) in 1993 and an M.Sc. in 1995 in Surveying Science from the University of Toronto. He is currently a Ph.D. candidate in the Department of Geodesy and Geomatics Engineering at the University of New Brunswick, where he is investigating the use of GPS for precise low-earth-orbiter tracking. Dr. Kim is a postdoctoral fellow in the same department, where he has been developing a new on-the-fly ambiguity resolution technique for long-baseline kinematic GPS applications and software for a gantry crane auto-steering system using the carrier-phase observations of high-data-rate GPS receivers. He has a B.Sc., an M.S., and a Ph.D. in geomatics from Seoul National University. He has been involved in GPS research since 1991 and is a member of the International Association of Geodesy Special Study Group, "Wide Area Modeling for Precise Satellite Positioning."*



To utilize the full measurement strength of the GPS carrier-phase observable for precise static or kinematic positioning, the integer ambiguities in the phase data must be removed. These ambiguities include both the initial integer ambiguities and the additional integer ambiguities introduced by cycle slips. For long-baseline kinematic data processing (with baseline lengths of hundreds or thousands of kilometers), it is very difficult to estimate the initial integer ambiguities and, if the data set is sufficiently long, researchers often leave them as real-valued estimates with little degradation in accuracy. However, accurate positioning requires the detection and full correction of cycle slips. This task can be quite labor intensive if using semi-automated techniques, or can produce erroneous results if implementing inappropriate automated techniques. Slip detection and repair still represents a challenge to carrier-phase data processing even after years of research, early on in which it was predicted that cycle slips would in all

likelihood not pose a problem in the future due to receiver advances.

The majority of approaches involve forming cycle slip-sensitive linear combinations of the available observables. Researchers have designed algorithms to detect, determine, and repair these cycle slips by fitting functions to the linear combinations and by observing differences between the functions and the data combinations. These methods invariably require user intervention for problematic cycle slips in portions of data, tuning of input parameters to data, or introduction of additional carrier-phase ambiguity-resolution parameters in the main data processing when preprocessing cycle-slip determination has failed.

In this article, we discuss the development of a cycle-slip detection and correction technique designed to detect and correct cycle slips in dual-frequency carrier phase data, in a fully automatic manner, utilizing carrier phase and pseudorange measurements in a postprocessing environment.

The prime objective of our work is to correctly detect and repair all cycle slips in the data preprocessing stage (sometimes referred to as the data editing stage), with straightforward algorithms independent of the quality of the input data.

### Detection and Determination

We begin our discussion with a general review of detection and determination philosophies, then expand on specific methods and equations.

**What is a cycle slip?** Briefly, it is a sudden jump of an integer number of cycles in the carrier phase observable, caused by the loss of lock of a receiver phase lock loop. The loss may be due to internal receiver tracking problems or to an interruption in the antenna's reception of satellite signals caused, for example, by a temporary signal blockage. A loss of lock may be shorter than the time interval between two adjacent data collection epochs or as long as the time interval between many epochs, in which case the term "data gap" may be in order. Correcting a cycle slip involves detecting it, estimating the exact number of L1 or L2 frequency cycles that comprise it, and actually correcting the subsequent phase measurements by this integer estimate.

For the most part, techniques used in the detection and determination of cycle slips have not changed significantly since the first methods were devised in the early 1980s. The focus has always been on attempting to develop a reliable, somewhat automatic detection and repair procedure. To detect a slip, a method must in some manner test at least one smooth (i.e., low-noise) quantity derived from the observations for discontinuities that may represent cycle slips.

The derived quantities usually consist of linear combinations of the undifferenced or double-differenced L1 and L2 carrier-phase and, possibly, pseudorange observations. Examples of combinations useful for kinematic data are the ionospheric phase delay, the range residual, and the widelane phase minus narrowlane pseudorange.

After producing the time series for the derived quantities, one can initiate the cycle-slip detection process. Of the various methods available, we will discuss here only four.

The most straightforward method is to compute higher-order time differences of the time series, which accentuate any discontinuities. Many static GPS data processing packages, including the University of New Brunswick's DIPOP (Differential POSitioning Program) software, use this approach. The main disadvantages of this method are that the user must set data-set-specific tolerance

values, and that kinematic data require geometry-free linear combinations.

Another method is to fit a low-degree polynomial over the time series and conclude that any large discrepancy between the polynomial and the time series represents a cycle slip. This method is also hampered by the number and size of slips altering the shape of the fitting polynomial.

A popular method, especially for kinematic data processing, where such filtering is used in the main processing stage, is Kalman filtering. An adjunct to this technique is the use of wavelets rather than Kalman filtering. The predicted time series values estimated from the developed dynamic model in the Kalman filter are compared with the actual data time series. Any statistically significant discrepancies are indicative of cycle slips. However, choosing appropriate filter parameters for the data set requires filter tuning and, if inappropriate parameter values are selected, the method can return unpredictable results, at least with undifferenced static data.

The final method we need to discuss consists, in part, of applying a running average filter to a linear combination to improve the estimate of the combination's ambiguity term. Cycle slips are detected by determining whether two consecutive unfiltered data points are outside the confidence interval of the running mean. This method and the Kalman filtering approach have the advantage of using statistical information from the data themselves in the detection process.

After detecting cycle slips, one must determine the actual number of L1 and/or L2 cycles that comprise each slip and then correct the data. The latter is a simple enough task, but the determination can require additional information. If one uses single-frequency linear combinations resulting in integer ambiguity values, then one can directly estimate the integer number of cycles attributable to the slip. If one uses a dual-frequency combination, then this single combination consists of two unknowns: the slip in L1 and the slip in L2. Therefore, solving uniquely for the individual frequency slips requires a second linear combination. This can be accomplished by using one of the detection methods on a second linear combination—not to detect a slip, but rather to estimate the inter-frequency slip. With this additional information, one can uniquely determine the values of the L1 and L2 cycle slips. Various techniques can fix the estimates to integers, ranging from simple rounding to searching for slip pairs that best fit the linear combinations in a least-squares sense. If one cannot determine viable integer combinations,

then one can introduce additional carrier-phase ambiguity resolution parameters in the main data processing.

## Automatic Cycle Slip Correction

Our technique represents an evolution, from static to kinematic and from semiautomatic to fully automatic data handling in the DIPOP preprocessors. After outlier detection and time-tag correction, the procedure forms two satellite-receiver, geometry-free linear combinations with the dual-frequency carrier phase and pseudorange measurements, for each baseline double-difference satellite pair. Various tests filter the noisier of the two combinations and detect cycle slips on each combination. The filtered combination is also filtered backwards and the data from the two combinations are used in a least-squares, polynomial fitting strategy to estimate the magnitude and sign of the double-difference L1 and L2 cycle slips in the time series. The estimated slips are applied in a correction routine. In order to verify correct determination, the procedure must then run a second round of identical detection. If it detects any residual slips, it re-initiates the determination and correction routines.

**Detection observables.** The detection observables are based on the double-differenced carrier-phase and pseudorange observables. For the L1 frequency, the double-differenced observables are

$$\begin{aligned} \nabla\Delta\Phi_1 &= \lambda_1 \nabla\Delta\phi_1 = \nabla\Delta\rho \\ &+ \nabla\Delta d_{\text{trop}} - \nabla\Delta d_{\text{ion}1} + \lambda_1 \nabla\Delta N_1 \\ &+ \nabla\Delta m_1 + \nabla\Delta\epsilon_1 \end{aligned} \quad (1)$$

and

$$\begin{aligned} \nabla\Delta P_1 &= \nabla\Delta\rho + \nabla\Delta d_{\text{trop}} \\ &+ \nabla\Delta d_{\text{ion}1} + \nabla\Delta M_1 + \nabla\Delta e_1 \end{aligned} \quad (2)$$

where  $\nabla\Delta$  is the double-difference operator;  $\Phi_i$  and  $P_i$  are the measured carrier phase and pseudorange (in distance units);  $\lambda_i$  is the carrier wavelength;  $\phi_i$  is the measured carrier phase (in cycles);  $\rho$  is the geometric range from the receiver to a GPS satellite;  $N_i$  is the number of cycles by which the initial phases are undetermined;  $d_{\text{trop}}$  and  $d_{\text{ion}1}$  are the delays due to the troposphere and the ionosphere;  $m_i$  and  $M_i$  represent the effect of multipath on the carrier phases and the pseudoranges; and  $\epsilon_i$  and  $e_i$  represent the effect of receiver noise on the carrier phases and the pseudoranges. We have ignored satellite and receiver hardware delays and other small effects, as they have negligible effect on data preprocessing. A similar expression can be written for the L2 frequency.

We chose two detection observables with minimal measurement noise and with the property that they do not contain any component of satellite-receiver range. Therefore, the two linear combinations produce time series that are relatively invariant to collection time, baseline separation, and static or kinematic data collection modes, within the limits of the residual ionosphere, multipath, and receiver noise. We chose the geometry-free phase combination and the widelane phase minus narrowlane pseudorange combination. We did not use the L1 and L2 range residuals, as the measurement noise terms of these observables are greater than that of the widelane phase minus narrowlane pseudorange combination. Different investigators have utilized both of the selected combinations for cycle-slip detection for undifferenced static data and for double-differenced short baseline static and kinematic data.

**Geometry-free phase.** The first observable is the geometry-free phase linear combination:

$$\begin{aligned} \lambda_1 \nabla\Delta\phi_1 - \lambda_2 \nabla\Delta\phi_2 &= (\nabla\Delta d_{\text{ion}2} - \nabla\Delta d_{\text{ion}1}) \\ &+ (\lambda_1 \nabla\Delta N_1 - \lambda_2 \nabla\Delta N_2) + (\nabla\Delta m_1 - \nabla\Delta m_2) \\ &+ (\nabla\Delta\epsilon_1 - \nabla\Delta\epsilon_2) \end{aligned} \quad (3)$$

This combination consists of inter-frequency double-difference ionosphere, L1 and L2 double-difference integer ambiguities, interfrequency double-difference phase multipath, and interfrequency double-difference receiver phase noise. A cycle slip on the next (post-slip) epoch of this combination would result in the ambiguities term in Equation 3 being replaced with

$$\lambda_1(\nabla\Delta N_1 + n_1) - \lambda_2(\nabla\Delta N_2 + n_2) \quad (4)$$

where  $n_1$  and  $n_2$  are the double-difference integer cycle slips (in cycles) on the L1 and L2 frequencies.

Figure 1 illustrates the behavior of this observable for a sample of data collected on

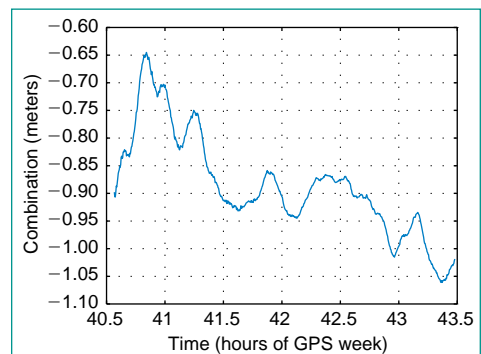


FIGURE 1 Variation in geometry-free phase combination.

# Innovation

a static baseline of approximately 200 kilometers. In the figure, we have differenced the geometry-free phase time series from the integer value of its first data point to remove the majority of the observable for which the ambiguity bias is the main constituent. We did this because the variation of the combination is the important aspect in this analysis. The variations are primarily due to the ionospheric term in Equation 3, whereas the phase multipath and noise terms have much higher frequencies and lower amplitudes.

**Widelane phase minus narrowlane pseudorange.** The second observable is the widelane phase minus narrowlane pseudorange linear combination:

$$\begin{aligned} & \lambda_4(\nabla\Delta\phi_1 - \nabla\Delta\phi_2) - \lambda_5\left(\frac{\nabla\Delta P_1}{\lambda_1} + \frac{\nabla\Delta P_2}{\lambda_2}\right) \\ &= \lambda_4(\nabla\Delta N_1 - \nabla\Delta N_2) \\ &+ \lambda_4\left(\frac{\nabla\Delta m_1}{\lambda_1} - \frac{\nabla\Delta m_2}{\lambda_2}\right) - \lambda_5\left(\frac{\nabla\Delta M_1}{\lambda_1} + \frac{\nabla\Delta M_2}{\lambda_2}\right) \quad (5) \\ &+ \lambda_4\left(\frac{\nabla\Delta\epsilon_1}{\lambda_1} - \frac{\nabla\Delta\epsilon_2}{\lambda_2}\right) - \lambda_5\left(\frac{\nabla\Delta e_1}{\lambda_1} + \frac{\nabla\Delta e_2}{\lambda_2}\right) \end{aligned}$$

where

$$\lambda_4 = \left(\lambda_1^{-1} - \lambda_2^{-1}\right)^{-1} \approx 86.2 \text{ centimeters}, \quad (6)$$

usually referred to as the widelane wavelength, and

$$\lambda_5 = \left(\lambda_1^{-1} + \lambda_2^{-1}\right)^{-1} \approx 10.7 \text{ centimeters} \quad (7)$$

usually referred to as the narrowlane wavelength.

This combination consists of the widelane ambiguity, a residual multipath term, and a residual receiver noise term; the ionospheric terms cancel (to first order).

Since the multipath and noise terms of the pseudorange measurements are much larger than those of the carrier phase measurements, the fluctuations in this combination are mainly due to pseudorange multipath and pseudorange measurement noise. The former of these error terms can cause quasi-sinusoidal variations of many meters. A cycle slip on the next (post-slip) epoch of this combination would result in the term with ambiguities being replaced with

$$\lambda_4\left[\left(\nabla\Delta N_1 + n_1\right) - \left(\nabla\Delta N_2 + n_2\right)\right] \quad (8)$$

The noise of this observable makes high resolution cycle-slip detection unlikely. However, use of a simple running average filter makes this observable more useful. This strategy is quite intuitive, since over

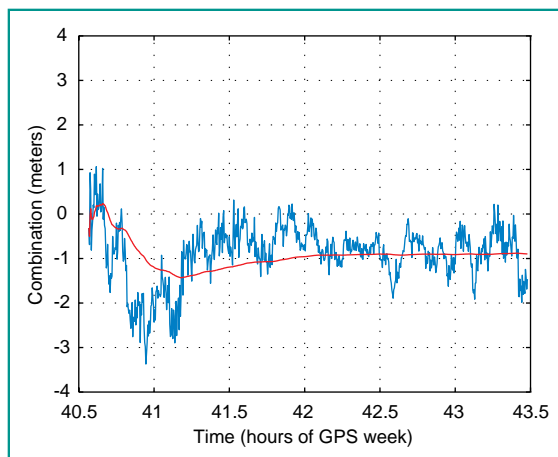


**FIGURE 2** Variation in widelane phase minus narrowlane pseudorange combination. The smooth line shows the running-average filtered values.

time one would expect the residual multipath and noise terms to average down to near-constant values. The filter is an expanding-memory, low-pass filter whose output is identical to the recursive mean:

$$\bar{x}_t = \bar{x}_{t-1} + \frac{1}{t} \left( x_t - \bar{x}_{t-1} \right) \quad (9)$$

where  $x$  is the observation,  $\bar{x}$  is the mean of  $x$ , and  $t$  and  $t-1$  represent the present and previous epoch counts, respectively.

**Figure 2** depicts this combination for the same data set used in Figure 1. The noise level is substantially higher than for the first combination, but this is tempered with the filtering. The running-average filtered results do not follow the raw data as well as, for example, a moving-average filter, especially due to the large degree of multipath at the start of the time series. But as long as there are no cycle slips, the running average is a better estimate of the ambiguity bias given these large errors.

## Detection Tests

Our procedure runs two different cycle-slip detection tests on each time series of the created combinations. It tests the geometry-free phase combination first, since that combination has the lower noise.

The first test investigates the variation of the time-normalized, between-epoch time difference of the geometry-free combination. **Figure 3** illustrates this quantity with the data from Figure 1. The principle used here is that a discontinuity in a time series is more pronounced in the time

differences of that series, since time differencing is analogous to high-pass filtering. From past experience with DIPOP, we implemented the comparison of a set of four time differences. The median time difference is differenced from the time difference value being tested. The absolute value of this difference leaves a very small component of the ionospheric, multipath, and noise terms, and an estimate of the cycle slip, if any, on this combination. The resulting value is differenced from a slip tolerance. In some software, one must select this tolerance on a data set-by-data set basis. In

the new approach we removed this human intervention by determining the time difference of the smallest type of cycle slip that can be observed consistently with this combination (from Equation 4), e.g.,

$$\begin{aligned} n_1 = 5, n_2 = 4 &\Rightarrow \left| \lambda_1 n_1 - \lambda_2 n_2 \right| \quad (10) \\ &\approx 2.5 \text{ centimeters} \end{aligned}$$

We will say more about this slip pairing and the choice of this pairing in the next section.

If the procedure detects a slip, then it carries out the second test. This test takes advantage of a property of time differencing: a discontinuity at one epoch will appear in the double time difference as two discontinuities adjacent in time.

For the widelane phase minus narrowlane pseudorange combination, the high noise level of the combination requires a different approach, namely a testing scheme modeled on one developed for undifferenced static data. The procedure

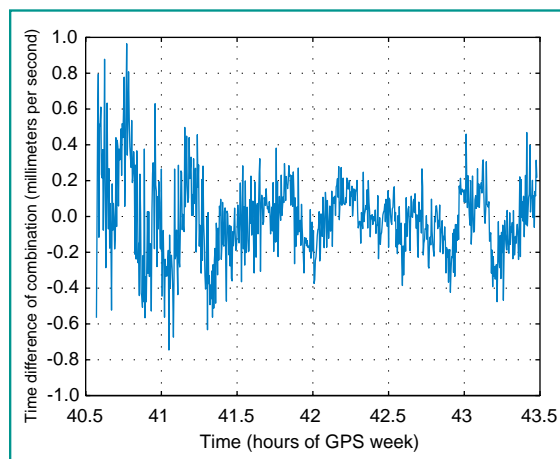


**FIGURE 3** Time difference of geometry-free combination.

filters the double-differenced measurements and compares the unfiltered data points with  $\pm 4\sigma$  of the filtered mean.

The recursive standard deviation is computed as

$$\sigma_t^2 = \sigma_{t-1}^2 + \frac{1}{t} \left[ \left( x_t - \bar{x}_{t-1} \right)^2 - \sigma_{t-1}^2 \right] \quad (11)$$

where  $\sigma$  is the biased sample standard deviation and the other variables are the same as those in Equation 9. The choice of the a priori variance value is not critical, as the recursive algorithm quickly determines variance values which are representative of the data set being processed.

The meaning of this test is that any value outside the expected ambiguity estimate (the running average confidence interval) at a data point represents a possible cycle slip. Unfiltered data from the previous and the subsequent epochs lying outside and within, respectively, one cycle of such a data point indicate a slip. One method of reducing the need for this second test could be to use a moving average and associated moving standard deviation. While the moving average would not be as good an estimate of the ambiguity bias, the moving standard deviation would better tolerate the effects of pseudorange multipath than the running standard deviation. Another option could be to utilize the receiver signal-to-noise values as an indicator of the combination noise.

Figure 4 illustrates a test of this approach. The unfiltered data are the same as in Figure 2, and we have added to the plot the  $\pm 4\sigma$  confidence intervals computed from Equation 11.

## Detection Insensitivity

Looking at Equations 4 and 8 individually, we note that the detection algorithms could miss many combinations of cycle slips ( $n_1$  and  $n_2$ ). However, the presented two-tiered approach greatly reduces the number of slip pairs to which both combinations are insensitive. From experience, we know that the geometry-free combination can be used to consistently detect cycle slips as small as a few centimeters, so we are concerned only with the combinations in TABLE 1. Other researchers have previously identified these

$n_1$	$n_2$	$n_1\lambda_1 - n_2\lambda_2$ (centimeters)	$(n_1 - n_2)\lambda_4$ (centimeters)
4	3	2.9	86.2
5	4	-2.5	86.2
9	7	0.3	172.4

TABLE 1 Critical combination-insensitive cycle-slip pairings.

situations, which represent the rationale for the slip tolerance set in the geometry-free phase detection tests. Later in this article we will discuss these slip pairs further.

## Determination

In order to precisely estimate the double-difference cycle slips in the given combinations, we integrated the geometry-free phase and widelane phase minus narrowlane pseudorange time series for each double-difference pair in a Chebyshev polynomial, least-squares fitting scheme.

To utilize the widelane phase minus narrowlane pseudorange combination, the procedure combines the forward and backward runs of the filter to optimally smooth the time series. The optimal smoothed estimate (unbiased and of minimum variance) is

$$\hat{x}_s(t) = C_s \left[ C_F^{-1} \hat{x}_F(t) + C_B^{-1} \hat{x}_B(t) \right], \quad (12)$$

$$C_s = \left( C_F^{-1} + C_B^{-1} \right)^{-1}$$

where the subscripts  $F/B$ , and  $S$  indicate forward filter, backward filter, and smoother, respectively;  $\hat{x}$  is the linear combination estimate; and  $C$  is the covariance matrix. The covariances for the forward and backward filters are estimated from Equation 11.

With noisier data we observed that the smoothing produced roughness at either end of the time series and on either side of detected cycle slips (the so-called "bow-tie" effect). This could cause errors in the slip estimation. To compensate for this, the procedure uses only data from the forward filter before a cycle slip and data from the backward filter after the slip.

The next step is the polynomial fitting. Chebyshev polynomial fitting was chosen for DIPOP, since it nearly completely minimizes the maximum residuals in the fit, making it a very robust technique. The procedure computes the Chebyshev polynomials on the basis of normalized time series time:

$$T_k(t) = \cos \left[ k \cos^{-1}(t) \right], \quad (13)$$

where  $T_k(t)$  is the  $k$ th Chebyshev polynomial base function at time  $t$ . The procedure then carries out a linear parametric least-squares fit of the polynomials to each linear data combination in order to estimate the Chebyshev polynomial coefficients and more

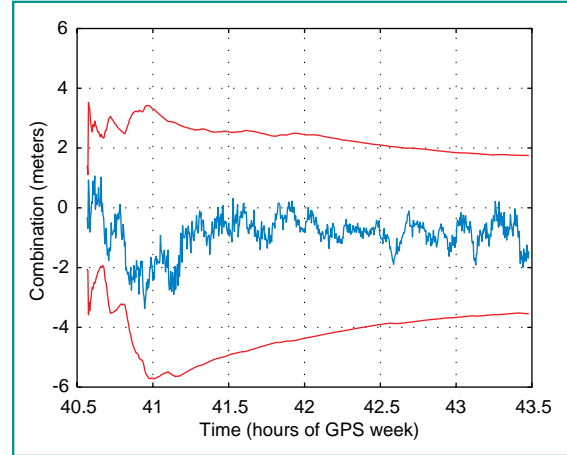


FIGURE 4 Variations in widelane phase minus narrowlane pseudorange combination with associated  $\pm 4\sigma$  confidence intervals.

importantly the estimates of the cycle slips in each combination. This is represented by

$$cs(t) + \sum_{k=1}^n T_{k-1}(t) C_k = obs(t), \quad (14)$$

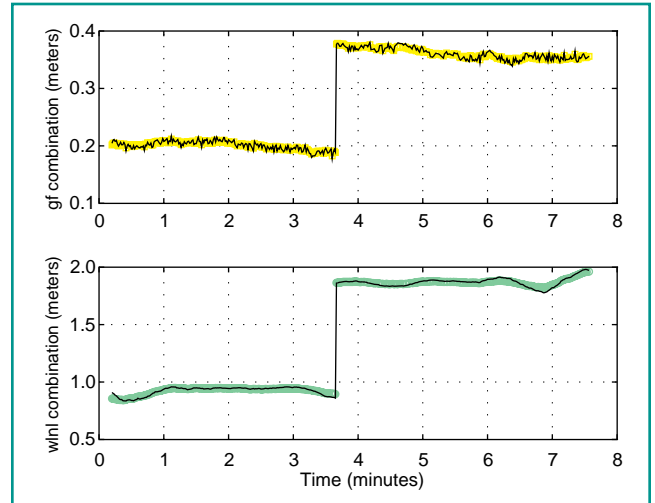
where  $cs$  is a cycle slip,  $T$  is a Chebyshev polynomial term,  $C$  is a polynomial coefficient, and  $obs$  is the time series value. From static DIPOP experience, one typically uses a polynomial of approximately order 30, but it may be appropriate to increase the order by making it a function of the number of epochs of data and the noise level of the widelane phase minus narrowlane pseudorange combination. The procedure estimates the combination cycle slips and the polynomial coefficients in a parametric least-squares adjustment along with the residuals of the least-squares fit. It then combines the combination slip estimates, the fit residuals, and the combination observations in a weighted parametric adjustment to estimate real-valued double-difference L1 and L2 cycle slips. Next, these results are rounded to obtain integer estimates.

Figure 5 illustrates an example of the determination procedure for a one-cycle cycle slip on L1. The differences in the fitted polynomials before and after the slip for each combination agree well with the theoretical values: 19.0 centimeters for the geometry-free phase and 86.2 centimeters for the widelane phase minus narrowlane pseudorange.

## Static Data Testing

In order to test the detection and determination strategy, we processed both static and kinematic data. We present the former here and the latter in the next section.

We deemed static data testing appropriate, since it allows for a "truth solution" to be determined with a semiautomated tech-



**FIGURE 5** Determination of cycle slip on geometry-free (gf) phase and widelane phase minus narrowlane pseudorange (wlnl) combinations. Thin lines represent combinations and thick, light lines represent fitted polynomials.

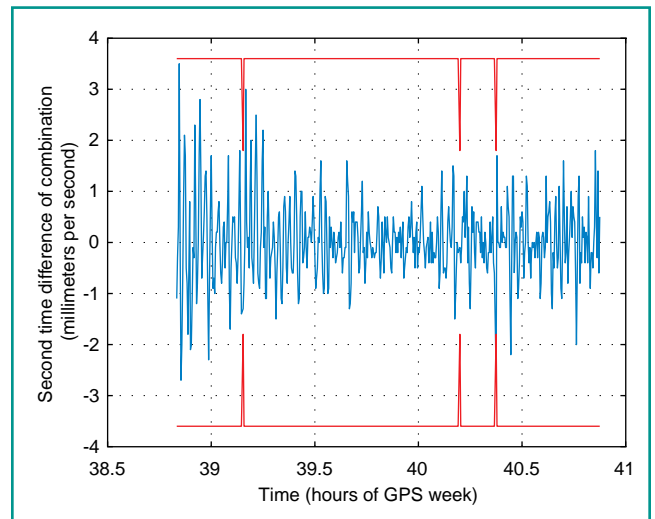


**FIGURE 6** Detected cycle slip in static data using geometry-free phase combination. The almost continuously horizontal lines are the slip tolerances for the first geometry-free phase detection test.

nique, using less noisy phase combinations in the cycle-slip correction process. The data set used is from a baseline of approximately 200 kilometers. The data contain a significant degree of multipath (as seen in Figures 1 and 2), which stem from ground and wall bounce multipath at one of the antenna locations. Such a corrupted data set is representative of an extreme environment and therefore provides a good test of robustness for our slip correction technique.

The results using this strategy produced the same detected and repaired cycle slips as with the manual processing strategy. The first geometry-free combination test detects a number of cycle slips erroneously, but the second test indicates from differencing that these apparent discontinuities are not true cycle slips. The widelane phase minus narrowlane pseudorange test does not incorrectly detect any slips, and the smoothing of these time series allows for precise estimation of the L1 and L2 slips. **Figure 6** shows an example of a detected slip. The slip can be observed at approximately 40.4

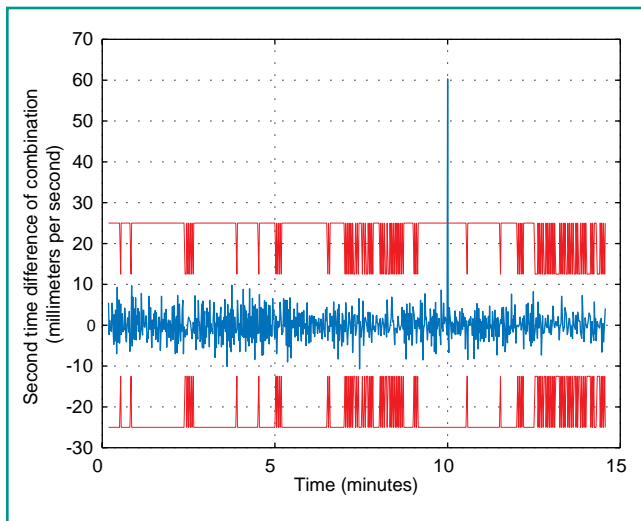


**FIGURE 7** Detected cycle slip in kinematic data using geometry-free phase combination.

hours on this time difference of the geometry-free combination. The slip is equal to two double-difference cycles on L1 and two double-difference cycles on L2, and therefore is not detectable on the widelane phase minus narrowlane pseudorange combination (see Table 1).

The above detection could become much more difficult during periods of large ionospheric fluctuations, when the ionospheric term represents the main noise contributor in the geometry-free phase combination. Others have indicated that a few-epoch moving average of the geometry-free phase combination subtracted from the actual combination can greatly reduce the effect of the ionospheric term, as long as the multipath is insignificant. Large discontinuities due to the changing ionospheric conditions should be avoided by using a high data collection rate.

## Kinematic Data Testing

The kinematic tests involved a marine situation, in which the vessel data were collected at an average distance of 40 kilometers from the reference receiver. This data set is representative of typical measurement conditions. The “truth solution” was obtained via a complex Kalman filtering procedure with manual verification. The results using the presented strategy compare favorably with the Kalman filtering results in that both processing techniques produce the same results.

Given that Table 1 indicates various problematic cycle-slip pairs, slip pairs of this kind were purposely injected into this kinematic data set to test the technique’s sensitivity. The results indicate that, with the tested data set, the most sensitive pairings described in

Table 1 can be detected and corrected with this technique. For example, the effect of the pairing  $n_1 = 5$ ,  $n_2 = 4$  can be clearly seen in Figure 7 at approximately 10 minutes. The time differencing of the geometry-free combinations greatly accentuates the slip and it can be detected unambiguously.

## Conclusions and Future Research

We have developed a completely automatic cycle-slip detection, determination, and

repair technique to preprocess dual-frequency, kinematic (and static) GPS data. The individual algorithms stem from research per-

formed by various authors and combined here in a novel procedure. The technique relies on the detection of cycle slips via two geometry-free linear combinations of the dual-frequency GPS measurements, namely the geometry-free phase and the widelane phase minus narrowlane pseudorange. A number of geometric and statistical tests detect slips for each combination. The results of these tests, when combined, represent a high-resolution, yet straightforward, method for detecting cycle slips. The determination of detected slips is performed by integrating the two combinations in a Chebyshev polynomial, least-squares fitting scheme.

Results using extremely noisy static and typical kinematic data, with both actual and simulated cycle slips, indicate that the technique is correctly detecting and repairing cycle slips (and needs only marginally increased processing time). Given that data sets vary significantly in the number and size of cycle slips and levels of ionospheric delay, multipath and noise, only more testing can further validate the performance of the technique. Possible improvements to the algorithms include the use of a moving standard deviation for detection on the widelane phase minus narrowlane pseudorange, and the use of receiver signal-to-noise values for the noise estimation. Determination may be improved with the use of fitting polynomials better tailored to the data and the use of other geometry-free combinations.

## Acknowledgments

Financial support for the work presented in this article was provided by the Natural Sciences and Engineering Research Council of Canada and the GEOIDE Network of Centres of Excellence. We would also like to thank the Canadian Hydrographic Service and the Canadian Coast Guard for providing the kinematic data set, and Paul Collins for processing one static data set that includes data from the United States Continuously Operating Reference Stations (CORS) network. This article is based on a paper presented at ION GPS 2000, the 13th International Technical Meeting of the Satellite Division of The Institute of Navigation, Salt Lake City, Utah, 19–22 September 2000. ☉

## Manufacturers

The test data illustrating this article were obtained using Z-12 receivers from **Ashtech Precision Products Division of Magellan Corporation** (Santa Clara, California) for the static test and a combination of an Ashtech Z-12 and 4000SSi receivers from **Trimble Navigation** (Sunnyvale, California) for the kinematic test.

## FURTHER READING

For further information on the carrier-phase observable, see

- ☉ “The GPS Observables” by R.B. Langley in *GPS World*, Vol. 4, No. 4, April 1993, pp. 52-59.
- ☉ “GPS Data Processing Methodology” by G. Blewitt in *GPS for Geodesy*, 2nd edition, edited by P.J.G. Teunissen and A. Kleusberg and published by Springer-Verlag, Berlin, 1998.
- ☉ *GPS Theory and Practice* by B. Hofmann-Wellenhof, H. Lichtenegger, and J. Collins, 4th Edition, published by Springer-Verlag, Vienna, 1997.

For a detailed review of cycle-slip detection algorithms, see

- ☉ “Cycle Slip Detection and Ambiguity Resolution Algorithms for Dual-Frequency GPS Data Processing” by Y. Gao and Z. Li in *Marine Geodesy*, Vol. 22, No. 4, 1999, pp. 169-181.

For a discussion of the sensitivity of different carrier phase combinations to cycle slips, see

- ☉ “An Overview of GPS Inter-frequency Carrier Phase Combinations” by J.P. Collins, an unpublished University of New Brunswick technical memorandum. An on-line version is available at <<http://gauss.gge.unb.ca/papers/pdf/L1L2combinations.collins.pdf>>.

For further details on the UNB cycle-slip handling approach, see

- ☉ “Efficient, Automated Cycle-slip Correction of Dual-frequency Kinematic GPS Data” by S.B. Bisnath in the *Proceedings of ION GPS 2000*, the 13th International Technical Meeting of The Institute of Navigation, Salt Lake City, Utah, 19–22 September 2000, pp. 145–154.